DATA AND ANALYSIS FROM A TIME-RESOLVED TOMOGRAPHIC OPTICAL BEAM DIAGNOSTIC*

Daniel K. Frayer[#], Douglas Johnson, National Security Technologies, LLC,
Los Alamos, NM 87544, U.S.A.
Carl Ekdahl, Los Alamos National Laboratory, Los Alamos, NM 87545, U.S.A.

Abstract

An optical tomographic diagnostic instrument developed for the acquisition of high-speed time-resolved images has been fielded at the Dual-Axis Radiographic Hydrodynamic Test (DARHT) Facility at Los Alamos National Laboratory. The instrument was developed for the creation of time histories of electron-beam cross section through the collection of Cerenkov light. Four optical lines of sight optically collapse an image and relay projections via an optical fiber relay to recording instruments; a tomographic reconstruction algorithm creates the time history. Because the instrument may be operated in an adverse environment, it may be operated, adjusted, and calibrated remotely. The instrument was operated over the course of various activities during and after DARHT commissioning, and tomographic reconstructions reported verifiable beam characteristics. Results from the collected data and reconstructions and analysis of the data are discussed.

INTRODUCTION

Kaufman et al. (2006) [1] describe design considerations for the development of a time-resolved diagnostic system for use at the Dual-Axis Radiographic Hydrodynamic Test (DARHT) Facility at Los Alamos National Laboratory. This design was finalized and the diagnostic instrument was fabricated, calibrated, and fielded. Frayer et al. (2008) [2] give the final system description and discuss characterization, qualification, integration, and preliminary experimental results.

In brief, the DARHT facility is designed to record high-speed radiographic images of explosively driven hydrodynamic events. This is accomplished by the illumination of a test object with x-ray pulses that occur within a 2 μs envelope and the recording of the resulting radiographic images. The x-ray pulses are generated by illuminating x-ray converter targets with high-power electron beams along two orthogonal axes.

The tomographic instrument was developed to create time histories of the DARHT electron beam when the DARHT second axis was being commissioned. Four discrete optical subsystems with distinct lines of sight view, through a 6-inch window in a pump cross, Cerenkov light generated by the beam incident upon a inside the vacuum envelope. Each subsystem employs cylindrical optics to image light in one direction and collapse light in the orthogonal direction. Each of the four

images and collapses in unique axes, thereby capturing information as a projection. Light along the imaging axes is relayed via optical fiber arrays and is recorded by streak cameras coupled to CCDs, resulting in temporal resolution of 2 ns over a recording window of 2 μs. Computer software then reconstructs a two-dimensional time history of the electron beam from the four optically collapsed one-dimensional (1-D) histories.

Two versions of this diagnostic have been built and fielded: a system with two lines of sight, as described by Bender et al. (2007) [3] and used in early stages of DARHT commissioning [4] and an earlier four-view system [5]. Both systems were fielded at DARHT in easily accessible, low-environmental-risk areas. This third-generation diagnostic was designed to be fielded in an area with restricted access and higher environmental risk, and to have the ability to change optical parameters during experiments. Although the optical design is similar to that of its predecessors, this instrument is necessarily more advanced as it offers remote calibration and remote control of optical magnification, focus, and aperture. This version of the instrument was fielded at DARHT in February, 2008, and has been operational since.
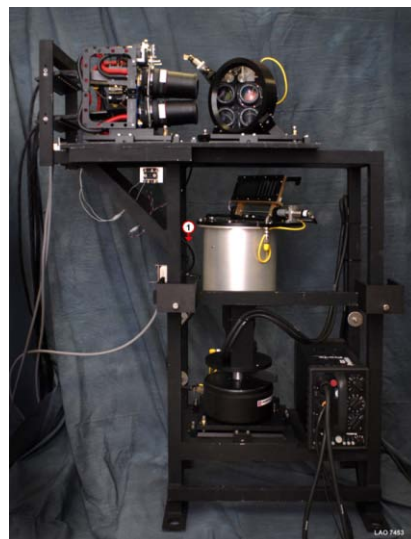

Figure 1: The DARHT tomographic instrument.

We first provide a brief treatment of the methodology used in reconstructing time-resolved images from the individual datasets. We give requirements upon the system for results of such reconstruction, as well as

qualification data proving system performance under the required condition. Finally, we analyze and discuss data from reconstructions of actual beam data.

TOMOGRAPHIC RECONSTRUCTION ALGORITHM

Given an image such as that given in Figure 2, a single-dimensional projection can be found at a given angle k by integrating in one direction at that angle. To simplify the notation, we can work in a rotated coordinate system:

$$s_k = x \cdot cos(\theta_k) + y \cdot sin(\theta_k) \qquad (1)$$

$$t_k = y \cdot cos(\theta_k) - x \cdot sin(\theta_k) \qquad (2)$$

The image then becomes the function $f(s_k, t_k)$, while the projection becomes

$$P_k(s_k) = \int f(s_k, t_k) \cdot dt_k \qquad (3)$$

In the case of the discussed system the actual image is unknown, and collected data consist of a number of projections at various angles. As such, the algorithm must proceed from the real data to a reconstruction of the original image. However, with a small number of projections there is no single solution. Given the smooth datasets expected from the accelerator, the maximum entropy constraint is added to force a unique solution:

$$H(f) = \iint f(x,y) \cdot ln(f(x,y)) \cdot dx \cdot dy$$
$$\Psi(f, \lambda) = H(f) + \sum_k \lambda_k(s_k) \cdot \left[P_k(s_k) - \int f(s_k, t_k) \cdot dt_k \right] \qquad (4)$$

with the function H(f) defined as the entropy of the image f(x,y). This entropy can be combined with the projection functions using LaGrange multipliers, λ_k, to form the functions Ψ_k. Differentiating with respect to the LaGrange multipliers and setting the result to zero returns the original definition of the projections:

$$\frac{d\Psi}{d\lambda} = \sum_k \left[P_k(s_k) - \int f(s_k, t_k) \cdot dt_k \right] = 0 \qquad (5)$$
$$P_k(s_k) = \int f(s_k, t_k) \cdot dt_k$$

Differentiating with respect to the image defines the image in relation to the LaGrange multipliers:

$$\frac{d\Psi}{d\lambda} = 1 + ln(f(x,y)) - \sum_k \lambda_k(s_k) = 0$$
$$f(x,y) = \epsilon \cdot e^{\sum_k \lambda_k(s_k)} \qquad (6)$$

Since the LaGrange multipliers are unknown, their exponentials are also unknown. We can simplify the result as:

$$f(x,y) = \prod_k h_k(s_k) \qquad (7)$$

This indicates that any given pixel in the reconstructed image is a product of the corresponding points in the h-functions. The h-functions have a one-to-one relationship to the projections as shown in Figure 3.
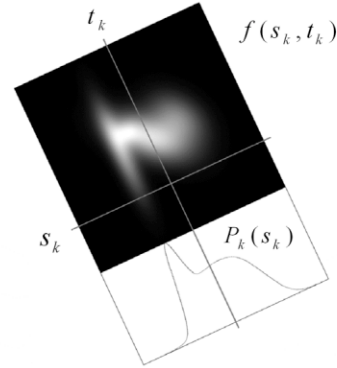

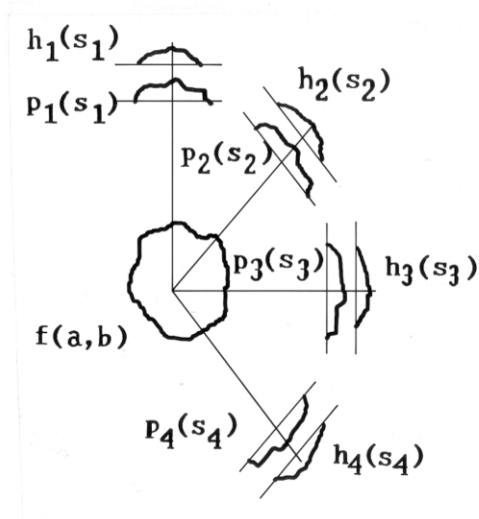Figure 2: A sample image and projection.

Figure 3: A sample image and projection.

The projection data are collected as a series of discrete points. The h-functions are found as a matching series of points. We can solve for the h-functions iteratively by starting with assumed values and adjusting them by comparing calculated projections with the data projections. Initially, all of the points in the h-functions are set equal to 1. An image is calculated from these and integrated to produce the calculated projections:

$$f(a, b) = \prod_k h_k(s_k(a, b))$$
$$P_{k,calc}(s_k) = \int f(s_k, t_k) \cdot dt_k \qquad (8)$$

New h-function values are then determined from the difference between the calculated and data projections:

$$h_{k,new}(s_k) = h_{k,old}(s_k) - \frac{g \cdot h_{k,old}(s_k) \cdot [P_{k,calc}(s_k) - P_{k,data}(s_k)]}{P_{k,calc}(s_k)} \qquad (9)$$

The variable g is a gain factor that is adjusted between 0 and 1. If set too high, the iterations become unstable and head towards infinity. If it is too low, the algorithm fails to converge. Iterations are manually repeated while gain factor is adjusted so that the difference between the calculated and data projections decreases sufficiently. Ideally the difference would converge to zero; in reality they will converge to some finite number, with the magnitude reflecting quality of the data.

Operationally, the reconstruction software has as inputs calibration images: per camera, a dark-field image with timing marks, a flat-field image and a resolution pattern; and two data files, one from each streak camera. As outputs, it produces the time-resolved series of images; each image or integrated set of images comes with calculated centroid position, RMS radius, skew, and kurtosis, each in x and y; and angle and ellipticity.

SYSTEM REQUIREMENTS AND QUALIFICATION

Initial customer requirements for the measurement of a beam profile elliptical in cross section and Gaussian in illumination profile to have the following accuracies [2]: 1) Centroid position to ±10% of radius for beam radii of 1 to 5 cm; 2) RMS radius to ±10% of radius for beam radii of 1 to 5 cm; and 3) Ellipticity (defined here as the ratio of minor and major axes) to ±10% of actual value for discernibly noncircular ellipses.

Optical requirements were determined by the system requirements [2]; the built instrument has a range of magnification, allowing a full field of view from 55.3 mm to more than 180 mm while operating at a distance of 0.5 m, with a resolution of 2.1 lp/mm in the high-magnification configuration. The functioning instrument was characterized in the laboratory with an illumination source as given in the requirements: namely, elliptical in cross section and with a Gaussian exitance profile. Calibrations were performed and five sets of data were taken of the ellipse while operating in a zoomed-in configuration. The tomographic reconstruction algorithm was applied to the data; results of ellipticity calculations are given in Figure 4, while an image of the original juxtaposed with a reconstruction is given in Figure 5.

RMS x and y radius calculations, based on five qualification runs and calculated with a 5% background, were 95.6% and 95.1% accurate, with standard deviations of 3.3% and 3.0%, respectively. Ellipticity calculations, based on the same reconstruction set, were 91.8% accurate, with a standard deviation of 0.97%. No absolute reference for centroid position was present, but x and y centroid position calculations had standard deviations of 0.72% and 12.0%, relative to RMS radius, respectively. Based on the results, the instrument received qualification and was fielded at DARHT in February, 2008.

BEAM DATA

The instrument operated during beam shots from February 2008 through February 2010. Data sets were
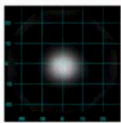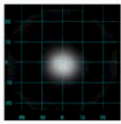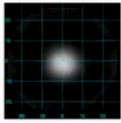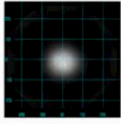
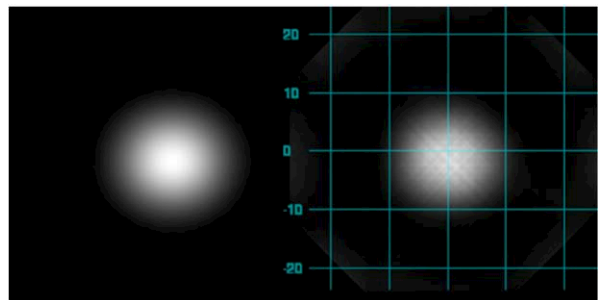Figure 4: Reconstructed ellipses for system qualification.

Figure 5: The illumination target (left) and reconstruction (right).

captured during 138 shots, and reconstructions were used in real-time to tune the DARHT beam line. Of these images, 44 were captured a) during shots in which the target was inserted into the beam line and b) simultaneously recorded by a PI-MAX single-frame camera imaging the reverse side of the beam target. Although data captured solely by the tomographic instrument are of value, for purposes of analyzing fidelity of capture and reconstruction, only data captured by both the tomographic instrument and the single-frame camera are useful. As such, only results from these 44 shots are analyzed here. As the majority of beam profiles were complex and highly nonelliptical, the assumption of ellipticity and Gaussian shape does not hold and quantitative error is expected. Also, as comparisons are being made to calculations from the PI-MAX images and such calculations are made with software that makes similar assumptions, the baseline numbers are themselves not expected to be entirely meaningful.
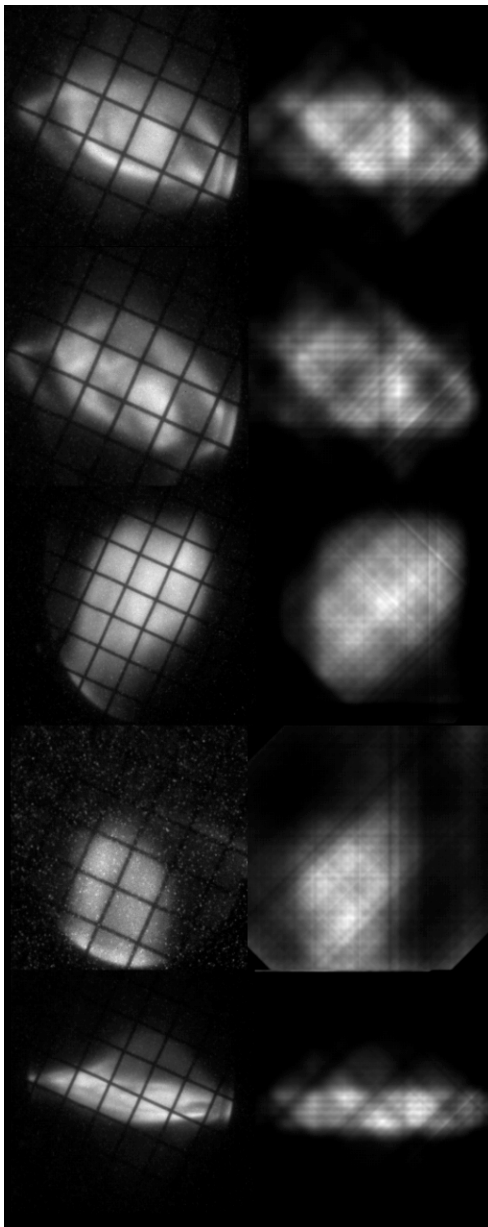
Figure 6: Selected correlated PI-MAX images (left) and tomographic reconstructions (right).

For each time record produced by the algorithm, images were integrated over the same temporal window, i.e., with the same initial time and duration, as that over which the PI-MAX recorded images in order to compare algorithmically produced measurements of centroid position (x and y), RMS radius (x and y) and ellipticity (here defined as the ratio between the difference in major and minor axes to the sum of the axes) for both images. Additionally, for each data set in which some pixels were saturated, an estimate for the ratio of saturated pixels to data pixels was made. This was done for the purpose of correlating error with saturation level, and was determined by counting pixels above an observable saturation threshold and those above a rough estimate of the background level. Representative pairs of temporally correlated PI-MAX images and reconstructed integrated

images are shown in Figure 6. Shown in Figures 7 through 9 are measured values of x centroid (Table 1), y centroid (2), x and y RMS radius (3) and ellipticity (4), respectively, along with calculated best fits.

ANALYSIS AND CONCLUSION

For all collected data, the tomographic instrument was fixed but the PI-MAX underwent several configuration changes, resulting in several subsets for both x and y centroid position with varying offsets. The data presented in Figure 7 have had these subtracted. For the charted datasets, best fits for x and y centroids were obtained by forcing equal slopes equal across data subsets while allowing offsets to vary. Those for x and y RMS radius were obtained by allowing the slopes to vary while maintaining offsets of zero. Both slope and offset were allowed to vary for ellipticity. Information derived from these figures is given in Table 1.

Several sources of error contaminate the original data and reconstructions. Background light affects both the PI-MAX camera and the tomographic system, although environmental and instrument configurations result in different levels seen by both in each correlated set, and changes in these configurations over the course of the entire dataset result in changes in background in a single instrument. Background is subtracted when making calculations from both raw images and reconstructions, but this process is not deterministic for the mentioned reasons. Additionally, light is generated in the fiber sub-arrays due to proximity to the beam line, in varying amounts due to relative placement. Finally, two current-return grids are present in the beam line, as can be seen in the left column of Figure 6, one seen by each system. These grids have different relative orientations, but more importantly, the one seen by the tomographic system is spatially separated from the beam target such that the four projections are contaminated with four different superpositions of the grid upon the target via parallax.

As can be seen in Table 1, the slopes for x and y centroid position, x and y RMS radius, and ellipticity are below unity such that lines with unity slopes are outside
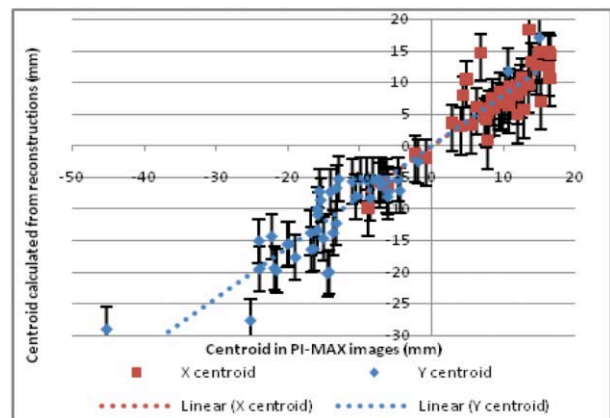

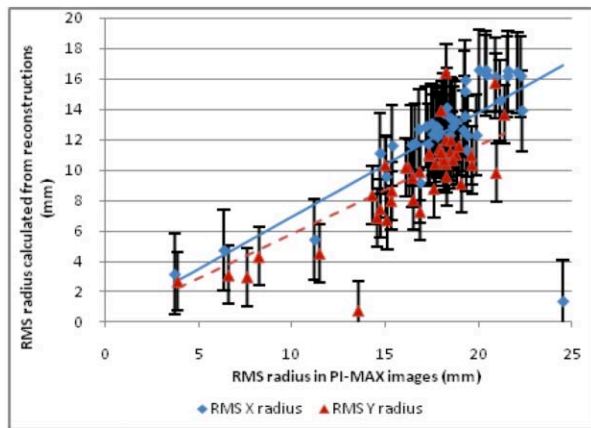Figure 7: Centroid x and y position with best fits.

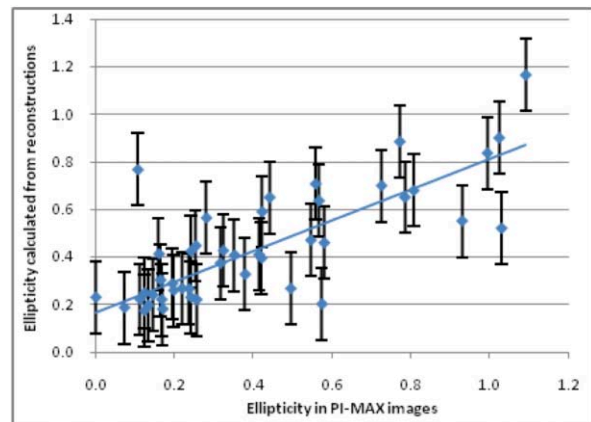Figure 8: RMS radius in x and y with best fits.

Figure 9: Ellipticity and best fit.

of the error bars for the calculations. As those calculated from datasets taken from elliptical sources are accurate, it is unclear whence the consistent inaccuracy in calculated radius of non-elliptical sources comes.

Compromise of data by saturation of pixels in one or more projections places the reconstruction in question. The convergence factor was found to correlate inversely

Table 1: Derived values from Figures 7−10

Figure	Datum	Value
7	X centroid slope	0.800
	X centroid offsets	2.89 mm
	X centroid standard deviation	0.801
8	X RMS radius slope	3.52
	X RMS radius standard deviation	0.689
	Y RMS radius slope	2.7 mm
	Y RMS radius standard deviation	0.582
9	Ellipticity slope	0.648
	Ellipticity offset	0.166
	Ellipticity standard deviation	0.2

with the ratio of data pixels saturated. However, error in any of the values listed in Table 1 was not found to correlate at all with this ratio. Unexpectedly, this was found to hold true even in severe cases of saturation, when blooming was induced on the streak-coupled CCD cameras, or when a large percentage of data pixels was compromised in multiple views. This implies a degree of robustness that is highly desirable in dynamic beam-tuning sequences, when it is not possible to predict light levels coming from the beam target and adjust the instrument accordingly ahead of time.

The described instrument and reconstruction software has proven a valuable tool in determining qualitative beam parameters such as temporally resolved movement, changes in shape, and note of features such as filamentation. It is expected that to be of value in determining quantitative values as the beam in DARHT second axis converges to the expected form. Future work on the tomographic instrument includes determination of consistent inaccuracy in calculated parameters in reconstructions of highly non-elliptical, non-Gaussian beam profiles relative to those calculated from imaged captured by the PI-MAX single-frame camera.

REFERENCES

[1] Kaufman, M., Frayer, D., Dreesen, W., Johnson, D., and Meidinger, A., "Design considerations for a time-resolved tomographic diagnostic at DARHT," Proc. SPIE 6289, 2006.

[2] Frayer, D., Cox, B., Dreesen, W., Johnson, D., Jones, M., Kaufman, M., "Fielding of a time-resolved tomographic diagnostic," Proc. SPIE 7061, 2008.

[3] Bender, H., Carlson, C., Frayer, D., Johnson, D., Jones, K., Meidinger A., Ekdahl, C., "Quasianamorphic optical imaging system with tomographic reconstruction for electron beam imaging," Rev. Sci. Instrum. 78(1), 013301 (2007).

[4] Ekdahl, E., Abeyta, O., Bender, H., Broste, W., Carlson, C., Caudill, L., Chan, K. C. D., Chen, Y. J., Dalmas, D., Durtschi, G., Eversole, S., Eylon, S., Fawley, W., Frayer, D., Gallegos, R., Harrison, J., Henestroza, E., Holzscheiter, M., Houck, T., Hughes, T., Jacquez, E., Johnson, D., Johnson, J., Jones, K., McCuistan, B. Trent, Meidinger, A., Montoya, N., Mostrom, C., Moy, K., Nielsen, K., Oro, D., Rodriguez, L., Rodriguez, P., Sanchez, M., Schauer, M., Simmons, D., Smith, H. V., Studebaker, J., Sturges, R., Sullivan, G., Swinney, C., Temple, R., Tom, C. Y., and Yu, S. S., "First beam at DARHT-II," Proc. of the 2004 Particle Accelerator Conference, 558−562 (2003).

[5] Ekdahl, E., Abeyta, E. O., Aragon, P., Archuleta, R., Bartsch, R., Bender, H., Broste, W., Carlson, C., Dalmas, D., Eversole, S., Frayer, D., Gallegos, R., Harrison, J., Jacquez, E., Johnson, D., Johnson, J., McCuistan, B. Trent, Montoya, N., Nath, S., Oro, D., Rowton, L., Sanchez, M., Scarpetti, R., Schauer, M., Seitz, G., Tipton, A., and Tom, C. Y., "Commissioning the DARHT-II scaled accelerator," Proc. of the 2007 Particle Accelerator Conference, 2373−5 (2007).